Fast-electron-impact study on excitations of $4p$, $4s$, and $3d$ electrons of krypton

Zhen-sheng Yuan,[1] Lin-fan Zhu,[1] Xiao-jing Liu,[1] Zhi-ping Zhong,[2] Wen-bin Li,[1] Hua-dong Cheng,[1] and Ke-zun Xu[1]
[1]*Laboratory of Bond Selective Chemistry, Department of Modern Physics, University of Science and Technology of China, Hefei, Anhui 230027, China*
[2]*Department of Physics, The Graduate School of the Chinese Academy of Sciences, P.O. Box 3908, Beijing 100039, China*
(Received 17 June 2002; published 6 December 2002)

Absolute optical oscillator strength densities for the excitations of the electrons $4p$, $4s$, and $3d$ have been measured. Their absolute optical oscillator strengths have also been obtained. An enhancement above the $4p$ ionization threshold in the photoabsorption spectrum was assigned as a delayed maximum which arises from the photoionization process of $4p \rightarrow \epsilon d$ according to present Dirac-Slater calculation. In the energy region of $4s$ autoionization, we have observed several features that are absent in previous fast-electron-impact work, but exist in optical measurements. We clarify this discrepancy here. Two Rydberg series of optically forbidden transitions, i.e., $4s^{-1}ns(^1S)$ $(n=5,6,7)$ and $4s^{-1}nd(^1D)$ $(n=4,5,6,7)$ have been observed when the spectrometer worked at conditions with larger momentum transfers, namely, $K^2=0.23$ a.u. and 0.67 a.u. Furthermore, the absolute optical oscillator strengths for the $3d$ excitation have been obtained.

DOI: 10.1103/PhysRevA.66.062701 PACS number(s): 34.80.Dp, 34.10.+x, 34.50.Fa

I. INTRODUCTION

The excitation properties of the krypton atom have been investigated extensively. Energy levels and cross sections are always essential contents of these investigations. To study these properties, different experimental techniques, including total photoabsorption, double-ion chamber, self-absorption, refraction index determination, phase-matching techniques, and electron-impact methods, have been used, which were reviewed by Chan *et al.* [1,2]. The theoretical relation between high-energy electron scattering and optical excitation has long been understood [3]. Both optical methods and electron-impact methods have their own advantages and shortcomings. For instance, it is hard to get proper oscillator strengths for discrete states by photoabsorption methods based on the Beer-Lambert law because of line-saturation effects [2], but fast electron-impact method is suitable for this purpose because of its nonresonant nature. Dipole(e, e) method was soon recognized as a very convenient approach to determine accurate optical oscillator strengths for a variety of atoms and molecules [2,4–12]. But on the other side, along with the significant advances in intensity and energy resolution of synchrotron radiation light sources, the optical method is taken as an important method to observe the ultrafine levels and high Rydberg series in the vacuum ultraviolet region [13].

Chan *et al.* gave a critical survey for the optical oscillator strengths (OOSs) of discrete states [1]. Till now, only three groups [1,14,15] have provided available OOS data for the discrete transitions of krypton at higher excitation energies by electron-impact-based methods, other than the usually measured $(^2P_{3/2})5s$ and $(^2P_{1/2})5s$ by the other experiments [16–25]. There are some differences for several transitions in their measured result. Using a semiempirical calculation, Geiger [14] reported the OOSs for these discrete states. There was an evident discrepancy between Geiger's calculation and the previous experiments.

For higher energies, namely, in the energy range 24–28 eV, the $4s \rightarrow np$ Rydberg series and some two-electron transitions have been observed, which are autoionization states [1,26–29]. The autoionization process was theoretically investigated by Fano, who gave a very compact formula to represent the interaction between a resonance and the continuum in the atomic (and molecular) spectra [30,31]. But his formula can only be used to analyze the spectrum with one isolated resonance. In order to describe the profiles of multiresonances in this energy region, Mies [32] and Shore [33] parametrized the cross section in different ways, which are theoretically equivalent [28].

Samson [26] obtained the spectrum in the $4s$ autoionization energy region for the first time by double-ion chamber technique. Then Fano and Cooper [31] took his spectrum as an example to illustrate their formula. Later, using synchrotron radiation method, Ederer [28], Codling and Madden [27], and Flemming *et al.* [29] studied these autoionization resonances and gave Shore's parameters for the resonant profiles. The agreement among these studies [27–29] is statisfying. But Samson's result [26] cannot be compared directly with that of the other three investigations because of different energy resolutions. Chan *et al.* [1] obtained the optical oscillator strength density spectrum (OOSDS) in this region by dipole (e, e) method and found that there was a resonance (at 24.73 eV) absent in their spectrum which appeared evidently in Samson's result [26]. So they assigned this resonance as peak ''Q.'' Till now, there has been no explanation for this discrepancy in previous studies. So we measured the spectrum and clarified these discrepancies as described in Sec. III B.

There are abundant optically forbidden transitions in this energy region, as studied by Brion and Olsen using threshold electron-impact spectra [34], and Baxter *et al.* using low-energy impact method [35]. In their studies, the optically allowed and forbidden transitions cannot be distinguished unambiguously because both these transitions appeared in the spectrum and overlapped seriously. Based on the fast-electron angle-resolved electron-energy-loss spectrometer (EELS), we can distinguish optically allowed and forbidden transitions as discussed in Sec. III B. So the energy levels, and sequentially the quantum defects of the two Rydberg

series of $4s^{-1}ns(^1S)$ $(n=5,6,7)$ and $4s^{-1}nd(^1D)$ $(n=4,5,6,7)$ have been determined in the present work.

In terms of $3d$ inner-shell excitations, King *et al.* [36] obtained energy levels and linewidths for states of $3d_{5/2}np$ and $3d_{3/2}np$ $(n=5,6,7,8)$ using EELS method, which has served a long time as the best reference for the linewidth of the resonantly excited states in rare gases. As a test for their modified SX-700 plane grating monochromater, Sairanen *et al.* [37] remeasured the same energy region as King *et al.* did by synchrotron radiation method and got more accurate linewidths for these states. As a complement for the information of this energy region, we achieved the absolute OOSs for the discrete states of $3d_{5/2}np$ and $3d_{3/2}np$ $(n=5,6,7)$ using EELS method.

Samson made a review of absorption spectra for the noble gases [38]. There were some nonhydrogenic features, such as minima or maxima, appearing in the spectra at the continuous energy regions. The phenomena of resonant and nonresonant maxima near threshold were discussed by Fano and Cooper [39]. They illustrated that for the electrons with a high angular momentum, e.g., d or f and so on, there may exist a double-well effective potential that comes from the combination of nuclear-electron attraction and centrifugal potential, and the maxima arise from the penetrating of these electrons, with certain energy, into the atom. In the case of krypton atom, Kennedy [40] reproduced the maxima observed by Samson [38] just above the first threshold with Hartree-Fock wave functions and gave the same interpretation as Fano and Cooper did [39]. Other theoretical studies [41–44] and experimental researches [1,45] also reported this phenomenon of maximum above ionization threshold, which was the ''delayed maximum,'' while they did not interpret this phenomenon in detail. Tong *et al.* [46,47] gave a more direct description of the relationship between the short-range phase shift of the final states and the delayed maxima, and the variation of the maxima position with respect to different atomic ionicities. In the present study, the delayed maximum just above the first ion threshold of krypton was measured by EELS method and interpreted by the Dirac-Slater (DS) approach [48–51].

II. EXPERIMENTAL AND THEORETICAL METHODS

An angle-resolved high-resolution fast-electron-energy-loss spectrometer (AREELS) was used in the present study. Detail of this spectrometer was described in Refs. [5,52,53]. Briefly, it consists of an electron gun, a hemispherical electrostatic monochromator made of aluminum, a rotatable energy analyzer of the same type, an interaction chamber, a number of cylindrical electrostatic lenses, and a one-dimensional position sensitive detector for gathering the analyzed electrons. All of these components are enclosed in four separate vacuum chambers made of stainless steel. In the present experimental measurements, this spectrometer was operated at an incident electron energy of 2.5 keV and an energy resolution of 60 meV full width at half maximum (FWHM). The sample of krypton gas was introduced into the gas cell in the center of the interaction chamber with the gas pressure of 8×10^{-3} Pa. The measured spectra were the sum

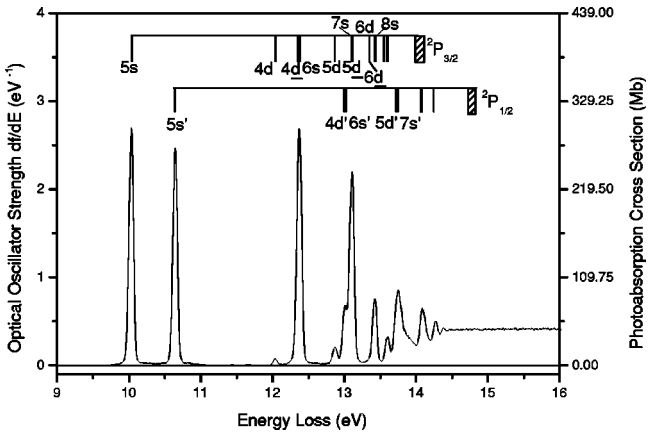

FIG. 1. Optical oscillator strength density spectrum for the discrete energy region. The assignments are taken from Ref. [55]. The $nd[\frac{1}{2}]$ and $nd[\frac{3}{2}]$ states which converge to the same $^2P_{3/2}$ limit are labeled as nd and $n\underline{d}$, respectively.

of many repetitive scans and the relative OOSDSs were established by multiplying the electron-energy-loss spectra by the known Bethe-Born conversion factor of the spectrometer. Absolute scales were obtained by normalizing optical oscillator strength density at 21.217 eV to Samson *et al.*'s result (38.31 Mb) [54] for the valence and inner-valence shell excitation, and at 96 eV to Chan *et al.*'s result (1.249 Mb) [1] for the inner-shell excitation. To identify the optically forbidden transitions, additional energy loss spectra were measured at 2° and 4° scattering angles.

The wave functions for the initial and final states were obtained by DS approach based on a self-consistent-field calculation [48–51] and the independent particle approximation. The quantum defects for the channels of $s_{1/2}$, $p_{1/2}$, $p_{3/2}$, $d_{3/2}$, and $d_{5/2}$ were obtained simultaneously. And then, the OOSDSs of transitions from the ground state to these channels were calculated on the level of first Born approximation. Considering the change of quantum defects [46,47] and the calculated OOSDSs, one can understand why there is a delayed maximum just above the $4p$ ionization threshold.

III. RESULTS AND DISCUSSION

A. In the energy region of valence shell excitations

The OOSDS for the discrete transitions is shown in Fig. 1 and the OOSs, which are achieved by a least-square fitting program, are tabulated in Table I with the previous electron-impact [1,14–16] and optical [17–25] studies. The estimated errors are listed in parentheses. The assignments of the energy levels are taken from Moore's table [55]. The $nd[\frac{1}{2}]$ and $nd[\frac{3}{2}]$ states which converge to the same $^2P_{3/2}$ limit are labeled as nd and $n\underline{d}$, respectively. For the energetically resolved peaks, such as $5s$, $5s'$, $4d$, $5d$, all of these four groups gave the close strengths. But for the unresolved peaks, discrepancies become larger. Nevertheless, the summation of OOSs for the unresolved peaks is coincident except for Geiger's results [14] (listed in Table II). So the discrepancies mentioned above may come from the fitting

TABLE I. Optical oscillator strengths for the valence shell excitations.

		Oscillator strengths (f)						
			Electron-impact method					
	Energy level (eV)	Theory Geiger[a]	Present work	Chan[b]	Geiger[a]	Natali[c]	Takayanagi[d]	Optical Methods
$(^2P_{3/2})5s$	10.033	0.250	0.214 (0.012)	0.214	0.195	0.212	0.143	0.155,[e] 0.208,[f] 0.187,[g] 0.21,[h] 0.204,[i] 0.159,[j] 0.166[k]
$(^2P_{3/2})6s$	12.385	0.108	0.147 (0.010)	0.154	0.142	0.152		
$(^2P_{3/2})7s$	13.114	0.0436	0.0808 (0.008)	0.113	0.187[l]	0.048		
$(^2P_{3/2})8s$	13.437	0.0163	0.0113 (0.0008)	0.0203	0.054[m]	0.0290		
$(^2P_{3/2})4d$	12.037	0.0144	0.0052 (0.0003)	0.0053	0.0055	0.0044		
$(^2P_{3/2})5d$	12.870	0.0114	0.0158 (0.0009)	0.0140	0.014	0.0138		
$(^2P_{3/2})6d$	13.350	0.0025	0.0042 (0.0003)	0.0015	0.0042	0.0024		
$(^2P_{3/2})4\underline{d}$	12.355	0.0973	0.093 (0.007)	0.0824	0.0649	0.0817		
$(^2P_{3/2})5\underline{d}$	13.099	0.0960	0.097 (0.010)	0.0610	0.187[l]	0.119		
$(^2P_{3/2})6\underline{d}$	13.423	0.0307	0.050 (0.004)	0.0439	0.054[m]	0.0295		
$(^2P_{1/2})5s'$	10.644	0.143	0.194 (0.012)	0.193	0.173	0.191	0.127	0.139,[e] 0.180,[n] 0.197,[f] 0.142,[o] 0.193,[g] 0.21,[h] 0.184,[i] 0.135[j]
$(^2P_{1/2})6s'$	13.037	0.0065	0.0079 (0.0008)	0.0105	0.015	0.0056		
$(^2P_{1/2})4d'$	13.005	0.0438	0.045 (0.003)	0.0435	0.0439	0.0420		
Total to ionization			1.120 (0.067)	1.126		1.10		

[a]Reference [14].
[b]Reference [1].
[c]Reference [15].
[d]Reference [16].
[e]Reference [17].
[f]Reference [19].
[g]Reference [21].
[h]Reference [22].
[i]Reference [23].
[j]Reference [24].
[k]Reference [25].
[l]The OOS summation of $7s$ and $5\underline{d}$.
[m]The OOS summation of $8s$ and $6\underline{d}$.
[n]Reference [18].
[o]Reference [20].

procedure. In order to clarify this problem, a higher-resolution experiment is needed. It seems that Geiger's semi-empirical calculation [14] is acceptable.

The OOSDS in the energy range 9–28 eV is shown in Fig. 2(a). It is interesting that there is a broad maximum just above the ionization threshold (14.00 eV), namely, at 16.3 eV, which shows significant nonhydrogenic behavior. In the continuum region, the quantum defect μ is equivalent to the short-range phase shift δ_l of the corresponding wave function with the relation of $\delta_l = \pi\mu$ [39,46,47]. The position of the delayed maximum in photoionization cross sections corresponds to the maximum of $2h\pi(d\mu/d\epsilon)$. Using DS method [48–51], we have calculated quantum defects for the orbitals $s_{1/2}$, $p_{1/2}$, $p_{3/2}$, $d_{3/2}$, and $d_{5/2}$, which are illustrated in Fig. 2(b). It can be seen that there is an evident increase of the quantum defects for the d-type orbitals in the energy range 0–5 eV above the threshold. This sharp change in quantum defects indicates that the wave functions at these energies have an abnormal behavior, so there may be a delayed maximum in the photoionization spectrum in this energy range [39,46,47]. The calculated optical oscillator strength densities for each channel are shown in Fig. 2(c). For the transitions of $4p_{1/2} \rightarrow \epsilon d_{3/2}$, $4p_{3/2} \rightarrow \epsilon d_{3/2}$, and $4p_{3/2} \rightarrow \epsilon d_{5/2}$, the energy positions of maxima are higher than the threshold. So the maxima appearing in present OOSD is expected arising from the photoionization progress of $4p \rightarrow \epsilon d$. The calculated total photoabsorption spectrum and the present experimental result are illustrated in Fig. 2(d). The calculated spectrum based on the DS theory decreases more sharply than the experimental result, which shows that configuration interaction will make photoabsorption distribution become diffused and shift to higher energies.

B. In the energy region of $4s$ autoionization

In this energy region, the spectra observed by Codling and Madden [27], Ederer [28], and Flemming *et al.* [29] have nearly the same features. The spectra of Samson [26] and Chan *et al.* [1] have lower energy resolutions and are different for some features. In Samson's [26] spectrum, there is a

TABLE II. The optical oscillator strengths for the unresolved peaks.

	Present	Chan *et al.*	Geiger	Natali *et al.*
f_{6s+4d}	0.240	0.236	0.207	0.239
f_{7s+5d}	0.178	0.174	0.187	0.167
$f_{6s'+4d'}$	0.053	0.054	0.059	0.048
$f_{6d+6d+8s}$	0.066	0.066	0.058	0.061

deep valley at 24.73 eV as shown in Fig. 3(a) (digitized data from Ref. [26]), while this feature does not appear in the study of Chan *et al.* [1]. As is well known, the electron-impact method is equivalent to optical method when the spectrometer works at the condition of optical limit approximation [3]. So the valley in Samson's [26] spectrum should be observed by Chan *et al.* [1] using EELS method, if it does exist. In order to clarify the discrepancies among previous investigations [1,26–29], we measured OOSDS in the 4*s* autoionization energy region using electron-impact method, which is shown in Fig. 3(b) as circles. Chan *et al.* did not observe the resonance at 24.73 eV, so they assigned it as peak "*Q*" [1]. But in Fig. 3(b), it is evident that there is a shallow well at 24.73 eV as well as another similar one at 25.18 eV. However, the peak "*Q*" is not as deep as shown in Fig. 3(a). It should be noted here that Chan *et al.*'s [1] energy resolution is 48 meV, Samson's [26] is ~120 meV, while that in the present work is 60 meV. In order to compare the present spectrum with the higher-resolution results [27–29], we constructed the photoabsorption spectrum considering Shore's parametrization of Codling *et al.* [27] and Flemming *et al.* [29], and convoluted the constructed spectrum by present spectrometer function, which is a quasi-Gaussian profile with 60 meV FWHM. Shore's parametrization is expressed as [33]

$$\sigma(E)=C(E)+\sum_{i}^{N}\frac{(E-E_i)(\Gamma_i/2)a_i+(\Gamma_i/2)^2 b_i}{(E-E_i)^2+(\Gamma_i/2)^2}, \quad (1)$$

where a_i, b_i have the dimension of a cross section and are proportional to the products of dipole and Coulomb matrix elements connecting the ground state with the continuum and

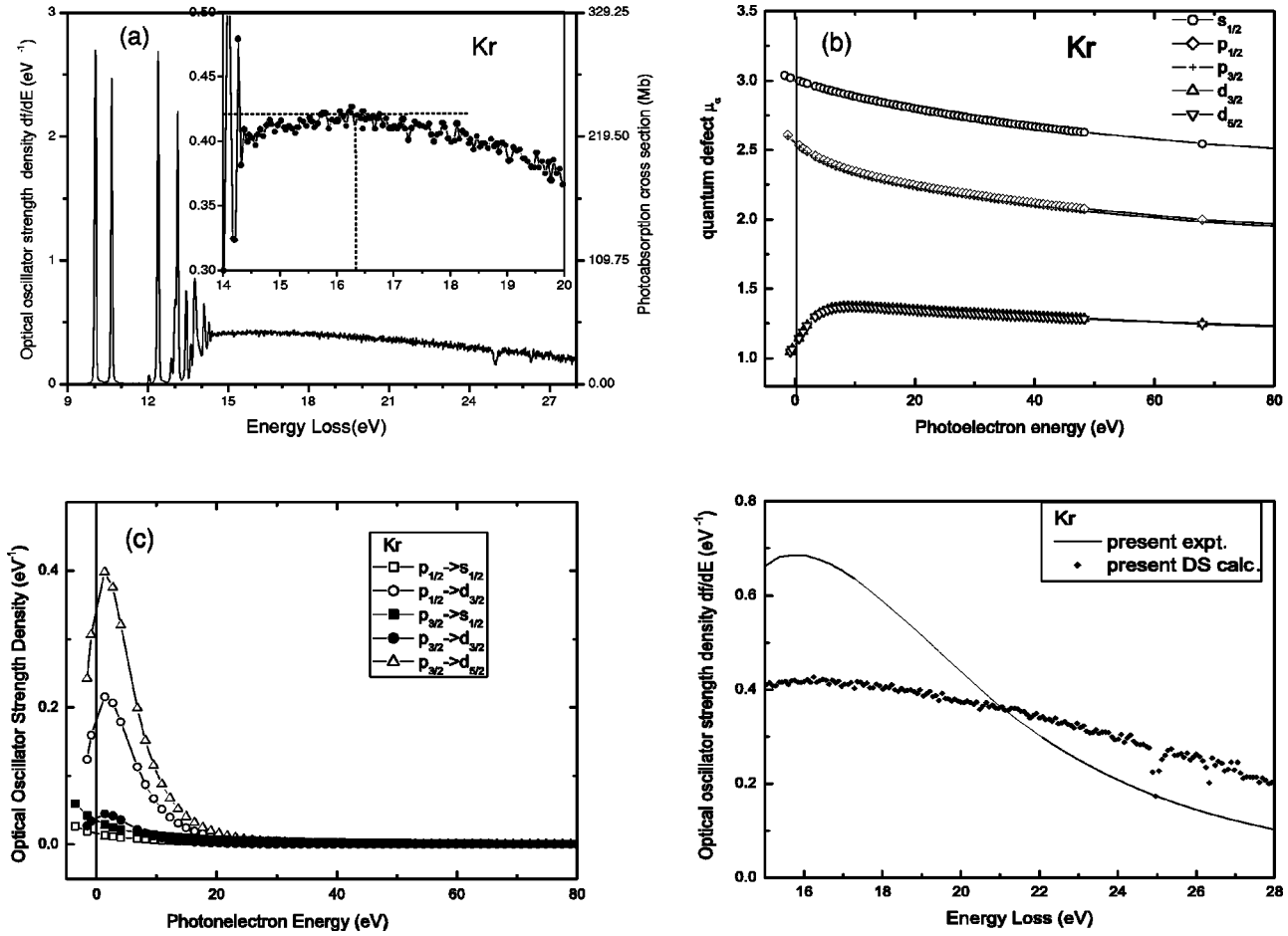

FIG. 2. Optical oscillator strength density spectrum and illustration for the delayed maximum. (a) The spectrum in the energy region 9–28 eV. The inset shows that there is a maximum at 16.3 eV. (b) The quantum defects calculated by DS theory. The quantum defects for $d_{3/2}$ and $d_{5/2}$ channels increase rapidly in the range of 0–5 eV above threshold. (c) The optical oscillator strength density for the five channels calculated by DS theory. It can be seen that the energy positions of the spectrum maxima for the three channels of $4p_{1/2}\rightarrow\epsilon d_{3/2}$, $4p_{3/2}\rightarrow\epsilon d_{3/2}$, and $4p_{3/2}\rightarrow\epsilon d_{5/2}$ are higher than the threshold. (d) The total optical oscillator strength density in the energy range 15–28 eV. The calculated result decreases more sharply than that in the present experiment.

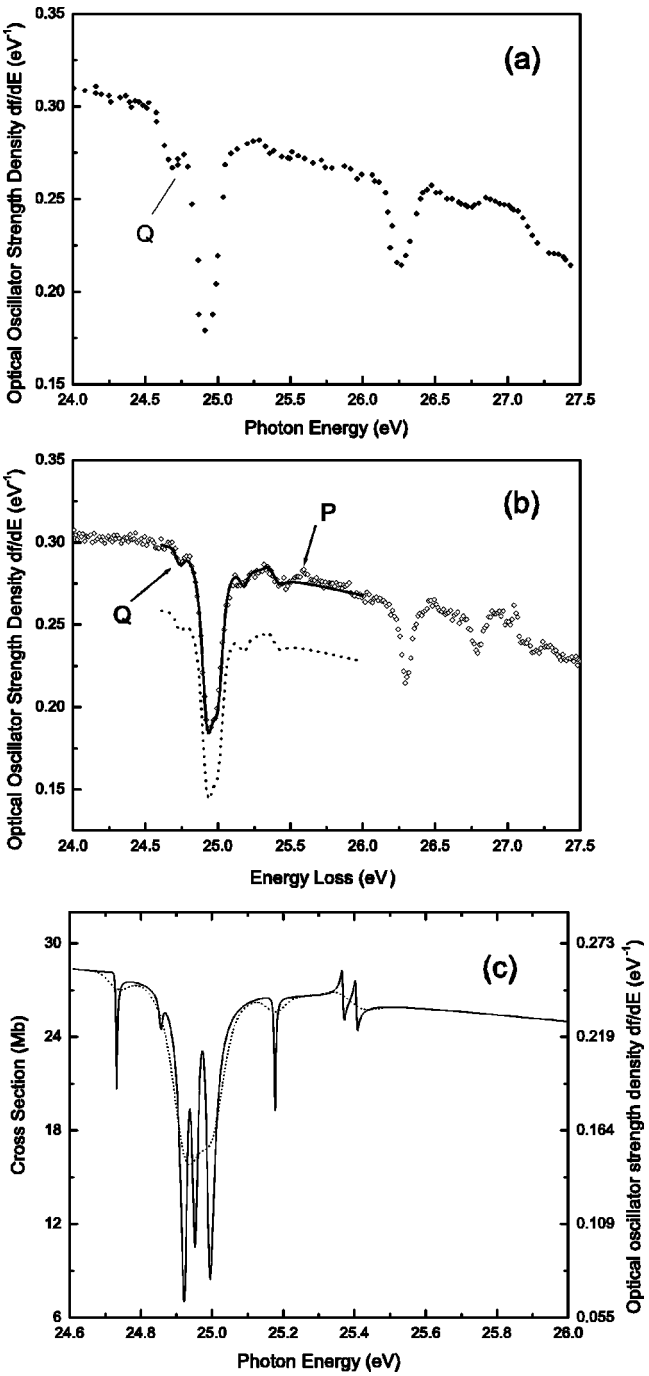

FIG. 3. Optical oscillator strength density spectrum in the energy region for the 4*s* autoionization. (a) Data points digitized from Ref. [26]. There is an evident valley at 24.73 eV, assigned as ''*Q*.'' (b) Circles, present experiment. Dashed line, constructed by Shore's parameters [27,29], after convoluted by present spectrometer function. Solid line, when the dashed line is moved up to present data. (c) Solid line, the spectrum constructed by Shore's parameters when Refs. [27,29] are considered. Dashed line, the convoluted result by present spectroscopy function, a Gaussian profile with 60 meV (FWHM).

the discrete excited state. Γ_i, E_i, and $C(E)$ are the resonance width, the resonance energy position, and the total background cross section, respectively. These parameters of a_i, b_i, Γ_i, and E_i are assumed to be energetically independent. While $a_i \rightarrow 0$, each term in the sum reduces to a simple Lorentzian profile. In this case, b_i is proportional to the oscillator strength between the ground state and the ith excited state, and inversely proportional to the resonance width Γ_i.

The convoluted data are plotted in Figs. 3(c) and 3(b) together with our experimental results. The dashed line is the convoluted result, which is slightly lower than the present spectrum because of different normalization resources [45,54]. When the dashed line is moved up to the solid line, it coincides with our spectrum excellently. Then the wells at 24.73 and 25.18 eV are related to the resonances 1 and 6 assigned by Codling [27], respectively, which are expected as two-electron excitations. The dip at 25.43 eV arises from the two resonances of 7 and 8 in Ref. [27]. A very weak peak at 25.63 eV assigned as ''*P*'' comes from the optically forbidden transition of $^1S_0 \rightarrow 4s^{-1}4d(^1D)$, because of our limited angle resolution, which will be discussed in the following paragraph. This agreement between Flemming *et al.*'s spectrum and ours indicates that: (a) electron-impact method is equivalent to optical method, (b) there may be some problem in Samson's spectrum [26] at 24.73 eV because the resonant well is much deeper than ours while their resolution is lower than ours. Why did Chan *et al.* [1] fail to observe the peak ''*Q*''? We guess that their event counts are not enough to stress the shallow well because of statistical uncertainty. After the spectrum constructed by Shore's parameters [29] was convoluted by the present spectrometer function, the ratio of the resonant depth to the magnitude of the flat region where it embodies in is about 1%. In other words, it needs at least 10^4 counts to make the shallow well visible. In present experiment, we accumulated about 4×10^4 counts for each energy point in this region. The other resonances appeared in Codling and Madden's [27] study can also be seen in the present spectrum as some shallow dips.

As mentioned in Sec. I, the electron-impact method can be used to identify the optically forbidden transitions at the condition of definite momentum transfer. Furthermore, in this region, the low-energy electron-impact spectrum is dominated by spin-forbidden-exchange-allowed transitions which would hinder observation of other types of optically forbidden processes, such as quadrupole or monopole transitions. However, in the fast-electron-impact spectra, even when the spectrometer works in the condition with higher momentum transfer, the spin-forbidden excitation is less important, while quadrupole-allowed excitations become more important [56]. Based on the fast-electron angle-resolved EELS, we can easily distinguish optically allowed and optically forbidden transitions. More specifically, when the spectrometer works at the optical limit, i.e., the momentum transfer $K \rightarrow 0$, the optical spectra can be observed. Then, the spectra will be measured at larger scattering angles, which means larger momentum transfers. At this moment, the optically forbidden transitions will arise. Therefore, it is helpful to assign different optically forbidden transitions through comparing the present fast-electron-impact spectra with previous low-electron-impact spectra. Through rotation of the analyzer, collision processes of varied momentum transfer can be observed as interpreted in detail by Zhong *et al.* [7],

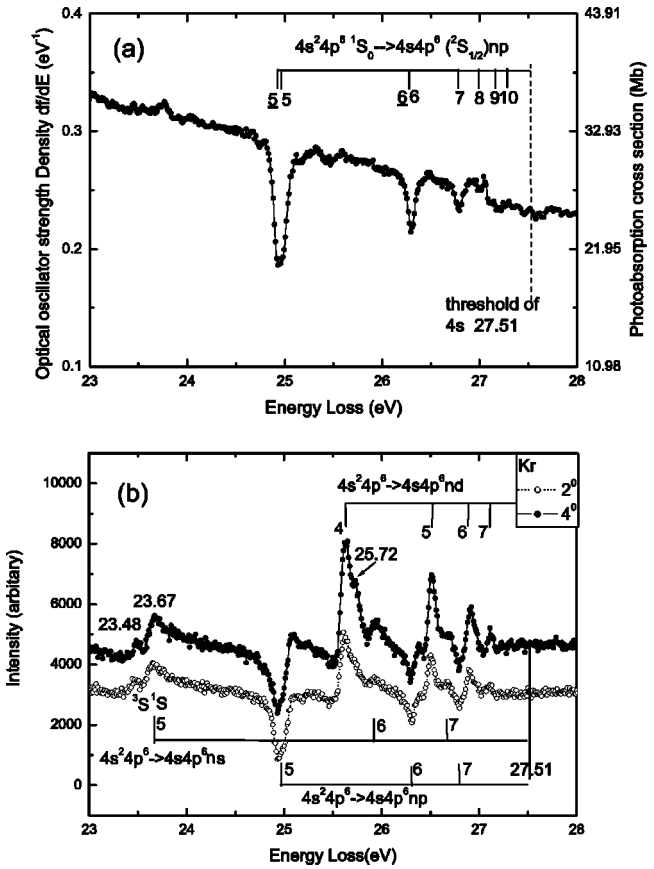

FIG. 4. Optically allowed and forbidden transitions. (a) The optical oscillator strength density spectrum. (b) Electron-energy-loss spectra in the same energy region measured at 2° and 4°, respectively. A straight line with definite slope, which is taken as the ionization background, was removed from the original spectrum.

Wu *et al.* [5], and Yuan *et al.* [57]. In the present experiment, we measured the electron-energy-loss spectrum at a 2500 eV impact energy and mean scattering angles of 2° and 4° (momentum transfer $K^2=0.23$ and 0.89 a.u.) and in the energy region 23–28 eV, which is shown in Fig. 4(b) accompanied by the OOSDS in Fig. 4(a). A straight line with definite slope, which is taken as smooth ionization background, has been subtracted from the energy-loss spectrum for each angle of 2° and 4° to make the comparison easier. It can be seen that a very weak peak arises around 23.75 eV in Fig. 4(a), which has not been mentioned in other optical researches [1,26–28]. In our previous studies on argon [5] and neon [7] under the same experimental conditions, similar features were found in electron-energy-loss spectra measured at 0°, which showed that optically forbidden transitions can be detected even when the momentum transfer square is smaller than 0.01 a.u. Therefore, this peak near 23.75 eV was supposed as an optically forbidden transition (present $K^2=0.0054$). By comparing Fig. 4(a) with Fig. 4(b), it is obvious that the ratios of areas for the peaks at 23.48 and 23.67 eV to the peak corresponding to $4s4p^65p$ optically allowed transition are much higher as the momentum transfer increases. Considering the energy positions of single excitations and the broad width of the two peaks [5,7], one can assign the two peaks to $4s4p^65s(^3S)$ and $4s4p^65s(^1S)$, respectively. Because spin-forbidden transitions should be much weaker than spin-allowed dipole-forbidden transitions in fast-electron-impact case [56], the peak at 23.48 eV is weaker than the peak at 23.67 eV. The Rydberg series shown in Fig. 4(b) can be classified into $4s^{-1}ns(^1S)(n\geqslant 5)$ and $4s^{-1}nd(^1D)(n\geqslant 4)$ as listed in detail in Table III, rather than classified into triplet states. The quantum defects for the two Rydberg series are also reduced out according to the Rydberg formula

TABLE III. The energy levels and effective quantum numbers for the Rydberg series of optically forbidden transitions.

	^1S			^1D		
Quantum number	Energy level (eV)	n^*	μ	Energy level (eV)	n^*	μ
4				25.63	2.69	1.31
5	23.67	1.88	3.12	26.52	3.70	1.30
6	25.94	2.94	3.06	26.90	4.72	1.28
7	26.66	4.00	3.00	27.12	5.91	1.09

$$E_n = I - \frac{13.6}{n^{*2}} = I - \frac{13.6}{(n-\mu)^2}. \tag{2}$$

It is obvious that the quantum defect μ becomes slightly smaller when the quantum number n is increased for both ^1S and ^1D states.

The width of the peak at 23.75 eV is smaller compared to that of $4s4p^65s$ (^1S and ^3S), and there is no single excitation corresponding to this peak, so it might be attributed to a two-electron transition. Similarly, the peak at 25.72 eV may come from a two-electron excitation as that assigned by Baxter *et al.* as "*J*" [35].

Fano [30] and Fano and Cooper [31] defined a factor of q to characterize the ratio of the transition probabilities to the "modified" discrete state Φ and to a bandwidth Γ of unperturbed continuum state Ψ_E. In the present spectrum, the resonant profiles of all the optically allowed transitions have a small $|q|$ factor while the resonant profiles of optically forbidden transitions have a large $|q|$ factor, which shows that the interactions between the optically allowed discrete states and the continua are stronger than those between the optically forbidden discrete states and the continua. From 2° to 4°, the intensity of optically forbidden transitions becomes relatively higher and the optically allowed transitions become more asymmetric rather than window resonant.

C. In the energy region of inner-shell 3*d* excitations

The OOSDS of 3*d* inner-shell excitations is shown in Fig. 5, in which the assignments are taken from King *et al.*'s study [36]. The relative OOSDS was normalized at 96 eV using Chan *et al.*'s [1] low-resolution data. We obtained the OOS's through the following procedure: first, a straight line

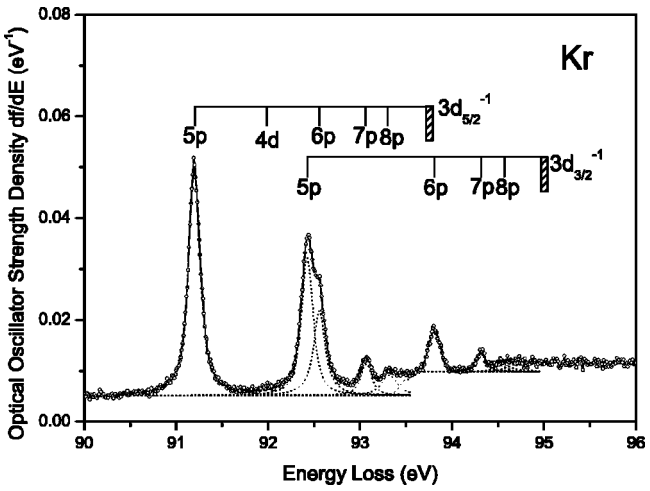

FIG. 5. Optical oscillator strength density spectrum in the energy region of $3d$ inner-shell excitations. Circles, experimental data; dotted lines, least-square-fitted curve. The assignments are taken from Ref. [36].

taken as the ionization background line was subtracted from the OOSDS, which has the magnitude of 0.0051 eV^{-1} as that at 89 eV; then the peaks of $3d_{5/2}^{-1}np$ $(n=5,6,7)$ and $3d_{3/2}^{-1}5p$ were deconvoluted using Voigt profiles. Similarly, the OOS's of $3d_{3/2}^{-1}np$ $(n=6,7)$ were obtained after the ionization background 0.0095 eV^{-1} was subtracted from the OOSDS. There is no previous absolute result that can be compared with the present OOSs. To compare with King *et al.*'s [36] relative generalized oscillator strength density df/dE, we determined df/dE by the following formula (in atomic unit) [36]:

$$\frac{df}{dE}=N^{*3}f_n. \tag{3}$$

As listed in Table IV, the absolute optical oscillator strengths of $3d_{5/2}^{-1}np$ and $3d_{3/2}^{-1}np$ $(n=5, 6, 7)$ are obtained and compared with King *et al.*'s relative generalized oscillator strength densities. The agreement is satisfying within the experimental errors, except for the state $3d_{3/2}^{-1}6p$. However, further absolute measurement is valuable because King *et al.*'s results are just relative.

IV. CONCLUSIONS

Using the AREELS method and DS calculation, we have investigated the discrete and continuum excitations and got the following results.

(1) The OOSs for discrete excitations of krypton have been determined by EELS method (illustrated in Fig. 1 and listed in Table I), and the agreement between the present observation and previous studies [1,14,15] is satisfying except for the unresolved and weak excitations, which indicate that a higher-resolution experiment is needed. The enhancement of the OOSDS at 16.3 eV (shown in Fig. 2) is a delayed maximum which stems from the photoionization of $4p \rightarrow \epsilon d$ according to the DS calculation.

(2) The discrepancies existing in previous EELS method and optical methods are clarified by the present work, which indicates that both EELS method and optical methods are equivalent. We observed the features that had been measured by other optical methods [26–29], which are shown in Fig. 3. The feature "*Q*" at 24.73 eV corresponds to feature 1 labeled by Codling *et al.* [27]. The reason why Chan *et al.* did not observe this resonance may be statistical uncertainty. Also, Samson's study [26] may give a misleading strength at this energy point.

(3) The energy levels of optically forbidden transitions of the two Rydberg series $4s^{-1}ns(^1S)$ $(n=5,6,7)$ and $4s^{-1}nd(^1D)$ $(n=4,5,6,7)$ are obtained as illustrated in Fig. 4 and listed in Table III. All the optically allowed transitions have a small $|q|$ factor, while optically forbidden transitions have a large $|q|$ factor at 2° and 4°, which indicates that the optically allowed resonances have stronger interactions with the continua than those of optically forbidden resonances. The theoretical investigation of these interactions is strongly recommended.

TABLE IV. Optical oscillator strengths for $3d$ excitations.

					Relative oscillator strength density	
		Level[a] (eV)	Effective quantum number[a] N^*	OOS Present (10^{-3})	Present[b]	King *et al.* [36]
$3d_{5/2}^{-1}$	$5p$	91.200	2.293	9.98(0.77)	1.0	1.0
	$6p$	92.560	3.330	3.84(0.34)	1.18(0.13)	1.16(4)
	$7p$	93.063	4.342	1.49(0.14)	1.01(0.12)	0.84(6)
	$8p$	93.301	5.348			1.06(45)
Edge		93.788				
$3d_{3/2}^{-1}$	$5p$	92.425	2.282	5.90(0.45)	0.58(0.06)	0.62(1)
	$6p$	93.809	3.319	1.79(0.13)	0.54(0.06)	0.71(4)
	$7p$	94.319	4.311	0.80(0.06)	0.53(0.06)	0.61(7)
	$8p$	94.567	5.337			0.45(18)
Edge		95.038				

[a]Energy levels and effective quantum numbers are taken from Ref. [36].
[b]The relative oscillator strength densities are normalized to the first transition $3d_{5/2}^{-1}5p$.

(4) The absolute OOSs for the $3d$ excitations are shown in Fig. 5 and tabulated in Table IV. Compared with King *et al.*'s relative generalized oscillator strengths [36], the agreement is satisfying except for one excitation. However, other absolute measurement is still valuable in order to compare with present absolute results.

ACKNOWLEDGMENTS

This work was supported by National Nature Science Fund of China (Grant Nos. 10134010, 10004010) and the Youth Foundation of the University of Science and Technology of China.

[1] W.F. Chan, G. Cooper, X. Guo, G.R. Burton, and C.E. Brion, Phys. Rev. A **46**, 149 (1992), and references therein.
[2] W.F. Chan, G. Cooper, and C.E. Brion, Phys. Rev. A **44**, 186 (1991).
[3] H. Bethe, Ann. Phys. (Leipzig) **5**, 325 (1930).
[4] T.N. Onley, N.M. Cann, G. Cooper, and C.E. Brion, Chem. Phys. **223**, 59 (1997).
[5] S.L. Wu, Z.P. Zhong, R.F. Feng, S.L. Xing, B.X. Yang, and K.Z. Xu, Phys. Rev. A **51**, 4494 (1995).
[6] K.Z. Xu, R.F. Feng, S.L. Wu, Q. Ji, X.J. Zhang, Z.P. Zhong, and Y. Zheng, Phys. Rev. A **53**, 3081 (1996).
[7] Z.P. Zhong, S.L. Wu, R.F. Feng, B.X. Yang, Q. Ji, K.Z. Xu, Y. Zou, and J.M. Li, Phys. Rev. A **55**, 3388 (1997).
[8] Z.P. Zhong, K.Z. Xu, R.F. Feng, X.J. Zhang, L.F. Zhu, and X.J. Liu, J. Electron Spectrosc. Relat. Phenom. **94**, 127 (1998).
[9] R.F. Feng, Q. Ji, L.F. Zhu, Q.C. Shi, S.L. Wu, X.J. Zhang, Z.P. Zhong, and K.Z. Xu, J. Phys. B **33**, 1357 (2000).
[10] X.J. Zhang, L.F. Zhu, Y.X. Wang, X.J. Liu, R.F. Feng, and K.Z. Xu, Chin. Phys. Lett. **16**, 882 (1999).
[11] A. Zecca, G.P. Karwasz, and R.S. Brusa, Riv. Nuovo Cimento **19**, 1 (1996); G.P. Karwasz, R.S. Brusa, and A. Zecca, *ibid.* **24**, 1 (2001); *ibid.* **24**, 1 (2001).
[12] A.P. Hitchcock, J. Electron Spectrosc. Relat. Phenom. **112**, 9 (2000).
[13] K. Schulz, G. Kaindl, M. Domke, J.D. Bozek, P.A. Heimann, A.S. Schlachter, and J.M. Rost, Phys. Rev. Lett. **77**, 3086 (1996).
[14] J. Geiger, Z. Phys. A **282**, 129 (1977).
[15] S. Natali, C.E. Kuyatt, and S.R. Miekzarek (unpublished), as quoted in Ref. [1].
[16] T. Takayanagi, G.P. Li, K. Wakiya, H. Suzuki, T. Ajiro, T. Inaba, S.S. Kano, and H. Takuma, Phys. Rev. A **41**, 5948 (1990).
[17] S. Tsurubuchi, K. Watanabe, and T. Arikawa, J. Phys. Soc. Jpn. **59**, 497 (1990).
[18] W.R. Ferrell, M.G. Payne, and W.R. Garrett, Phys. Rev. A **35**, 5020 (1987).
[19] E. Matthias, R.A. Rosenberg, E.D. Poliakoff, M.G. White, S.T. Lee, and D. A. Shirley, Chem. Phys. Lett. **52**, 239 (1977).
[20] J.P. De Jongh and J. Van Eck, Physica (Amsterdam) **51**, 104 (1971).
[21] P.M. Griffin and J.W. Hutchson, J. Opt. Soc. Am. **59**, 1607 (1969).
[22] G.I. Chashchina and E.Ya. Shreider, Opt. Spectrosc. **22**, 284 (1967).
[23] E.L. Lewis, Proc. Phys. Soc. London **92**, 817 (1967).
[24] P.G. Wilkinson, J. Quant. Spectrosc. Radiat. Transf. **5**, 503 (1965).
[25] R. Turner, Phys. Rev. **140**, A426 (1965).
[26] J.A.R. Samson, Phys. Rev. **132**, 2122 (1963).
[27] K. Codling and R.P. Madden, J. Res. Natl. Bur. Stand., Sect. A **76**, 1 (1972).
[28] D.L. Ederer, Phys. Rev. A **4**, 2263 (1971).
[29] M.G. Flemming, J.Z. Wu, C.D. Caldwell, and M.O. Krause, Phys. Rev. A **44**, 1733 (1991).
[30] U. Fano, Phys. Rev. **124**, 1866 (1961).
[31] U. Fano and J.W. Cooper, Phys. Rev. **137**, A1364 (1965).
[32] F.H. Mies, Phys. Rev. **175**, 164 (1968).
[33] B.W. Shore, Phys. Rev. **171**, 43 (1968).
[34] C.E. Brion and L.A.R. Olsen, J. Phys. B **3**, 1020 (1970).
[35] J.A. Baxter, P. Mitchell, and J. Comer, J. Phys. B **15**, 1105 (1982).
[36] G.C. King, M. Tronc, F.H. Read, and R.C. Bradford, J. Phys. B **10**, 2479 (1977).
[37] O.P. Sairanen, A. Kivimäki, E. Nõmmiste, H. Aksela, and S. Aksela, Phys. Rev. A **54**, 2834 (1996).
[38] J.A.R. Samson, Adv. At. Mol. Phys. **2**, 177 (1966).
[39] U. Fano and J.W. Cooper, Rev. Mod. Phys. **40**, 441 (1968).
[40] D.J. Kennedy and S.T. Manson, Phys. Rev. A **5**, 227 (1972).
[41] E.J. McGuire, Phys. Rev. **175**, 20 (1968).
[42] A. Zangwill and P. Soven, Phys. Rev. A **21**, 1561 (1980).
[43] W.R. Johnson and K.T. Cheng, Phys. Rev. A **20**, 978 (1979).
[44] F.A. Parpia, W.R. Johnson, and V. Radojevic, Phys. Rev. A **29**, 3173 (1984).
[45] G.V. Marr and J.B. West, At. Data Nucl. Data Tables **18**, 497 (1976).
[46] X.M. Tong, J.M. Li, and R.H. Pratt, Phys. Rev. A **42**, 5348 (1990).
[47] X.M. Tong, Acta Phys. Sin. **40**, 693 (1991).
[48] I.P. Grant, Adv. Phys. **19**, 747 (1970).
[49] J.M. Li and Z.X. Zhao, Acta Phys. Sin. **31**, 97 (1982).
[50] Q.C. Shi, S.M. Zhang, H. Cho, K.Z. Xu, J.M. Li, and S. Kais, J. Phys. B **31**, 4123 (1998).
[51] Q.C. Shi, K.Z. Xu, Z.J. Chen, H. Cho, and J.M. Li, Phys. Rev. A **57**, 4980 (1998).
[52] R.F. Feng, B.X. Yang, S.L. Wu, S.L. Xing, F. Zhang, Z.P. Zhong, X.Z. Guo, and K.Z. Xu, Sci. China, Ser. A: Math., Phys., Astron. **39**, 1288 (1996).
[53] X.J. Liu, L.F. Zhu, X.M. Jiang, Z.S. Yuan, B. Cai, X.J. Chen, and K.Z. Xu, Rev. Sci. Instrum. **72**, 3357 (2001).
[54] J.A.R. Samson and L.F. Yin, J. Opt. Soc. Am. B **6**, 2326 (1989).
[55] C.E. Moore, *Atomic Energy Levels* (U.S. GPO, Washington, D.C., 1952), Vol. 2.
[56] C.R. Brundle and A.D. Baker, *Electron Spectroscopy: Theory, Techniques and Applications* (Academic Press, London, 1979), Vol. 3, p. 177.
[57] Z.S. Yuan, L.F. Zhu, X.J. Liu, W.B. Li, H.D. Cheng, and K.Z. Xu, Chin. Phys. Lett. **19**, 495 (2002).